Mechanical behaviour of compacted kaolin clay stabilised via alkali activated calcium-rich fly ash binder

Elodie Coudert, Giacomo Russo, Dimitri Deneele, Alessandro Tarantino

Author's original manuscript published in Geomechanics for Energy and the Environment, 32(2022)
https://doi.org/10.1016/j.gete.2022.100404

SUBMISSION TO
JOURNAL OF GEOMECHANICS FOR ENERGY AND THE ENVIRONMENT
SPECIAL ISSUE ON 'LOW CARBON GEOTECHNICS'

DATE:
Written: July 2021

TITLE:
Mechanical behaviour of compacted kaolin clay stabilised via alkali activated calcium-rich fly ash binder

AUTHORS:
Elodie Coudert[a,b,c]
Dimitri Deneele[c,d]
Giacomo Russo[e],*
Alessandro Tarantino[b]

AFFILIATION:
[a]Department of Civil and Mechanical Engineering. University of Cassino and Southern Lazio, Via G. Di Biasio 43. 03043 Cassino, Italy
[b]Department of Civil and Environmental Engineering, University of Strathclyde, 75 Montrose Street, Glasgow, Scotland, G1 1XJ, United Kingdom
[c]Institut des Matériaux Jean Rouxel (IMN), Université de Nantes, CNRS, 2 rue de la Houssinière, BP 32229, 44322 Nantes Cedex 3, France
[d]GERS-LEE, Univ Gustave Eiffel, IFSTTAR, F-44344 Bouguenais, France;
[e]Department of Earth Science, Environment and Resources, University of Napoli Federico II, Via Cinthia 21 80126, Napoli, Italy

*CORRESPONDING AUTHOR:
Prof Giacomo Russo
Department of Earth Science, Environment and Resources,
University of Napoli Federico II
Via Cinthia 21 80126, Napoli, Italy
E-mail: giarusso@unina.it.

KEYWORDS
Soil stabilisation
Alkali activated material
Kaolin
Fly ash
Mechanical behaviour
Microstructure

Abstract

Locally sourced marginal earthfill geomaterials are generally not used in traditional earthfill construction due to their relatively poor mechanical performance. However, if these geomaterials are stabilised, procuring and transporting of materials from borrow sites can be avoided with significant carbon saving. Further carbon saving can be achieved by using industrial waste as binder in place of conventional high-carbon footprint stabilisers such as lime and Ordinary Portland Cement. This paper examines the use of a calcium-rich fly ash from coal combustion activated by a sodium-based alkaline solution for the treatment of non-active clay in view of its use as earthfill geomaterial. To this end, kaolinite clay/fly ash (90/10) samples were compacted, cured for different periods, saturated, and subjected to one-dimensional compression and direct shear tests. The major outcome from 1D compression tests is that stiffness is enhanced significantly even in the very short-term (1 day after alkali activation), i.e. before the binding phase starts to form. This was attributed to the changes in pore-water chemistry (increase in pH and electrolyte concentration) following the addition of the alkaline solution and the formation of aggregates in face-to-face mode. In the long term (curing time ≥28days) stiffness appeared to be further enhanced due to the formation of the binding phase. These effects were more pronounced in the low-intermediate stress range (<~700 kPa) making the alkali activation a good soil treatment for roadway embankments. Peak shear strength also appeared to be significantly enhanced in both short and long term although effects were more pronounced for curing time ≥28days following the formation of the binding phase. Ultimate shear strength is enhanced only in the long term (curing time ≥28days).

Mechanical behaviour of compacted kaolin clay stabilised via alkali activated calcium-rich fly ash binder

Coudert E, Deneele D, Russo G, Tarantino A

1 Introduction

Soft clay-rich soils are often encountered in construction sites. These soils cannot be directly used as earthfill materials and may cause problems in earthworks because of their poor mechanical performance. To improve their engineering characteristics Ordinary Portland Cement or lime are commonly used as soil stabilisers. These are associated with high carbon dioxide emissions and energy intensive processes, which increase significantly worldwide carbon footprint (Scrivener and Kirkpatrick, 2008). As a substitute, the use of Alkali Activated Materials (AAM) has received increasing attention over the last decade. In fact, AAMs present a much lower CO_2 emission process compared to traditional Portland cement (Provis and van Deventer, 2014). Recent studies have proved that alkali activated binders can be used successfully for stabilisation of a wide range of soils including clayey soil (Wilkinson et al., 2010; Singhi et al., 2016), sandy clay (Cristelo et al., 2011), marl, marlstone (Cristelo et al., 2012), silty sand (Rios et al., 2016) and road aggregates (Tenn et al., 2015). Applications have included deep soft soil improvement (Cristelo et al., 2011) and rammed earth construction (Silva et al., 2013).

However, these studies have mainly focused on soil-fly ash samples prepared form slurry state. When compacted fly ash samples were tested, investigation of mechanical properties was limited to unconfined compressive strength (UCS).

To investigate whether alkali activated fly ash can be potentially used to stabilise marginal clays in turn to be used as construction material for earth structures, compressibility and shear strength properties should be tested. From a practical point of view, the time scale of the effects of alkali activation should also be investigated as this affects the construction process and the time required for the embankments to come into service after construction.

This paper presents an experimental investigation of the mechanical behaviour of compacted clay stabilised with alkali activated fly ash. Oedometer and direct shear tests were carried out to investigate compressibility and shear strength of the clay-fly ash mixtures, which were compacted and then cured for different periods following alkali activation. Mercury intrusion porosimetry tests were also conducted to investigate microstructural features of samples prepared by mixing clay and alkali-activated fly ash.

A calcium-rich fly ash from coal combustion was used in this study, which was activated by a sodium-based alkaline solution. Kaolin was selected as its reactivity to alkaline activation at ambient temperature is negligible, and hence it does not interfere in the reaction sequence allowing for a study of the binder effect only. Besides, kaolin represents a wide class of clays encountered in engineering projects and so it is considered here as a model soil.

2 Background

Alkali Activated Materials derive from the reaction between solid aluminosilicate powder (usually metakaolin, fly ash, blast furnace slag or natural pozzolan) and alkali metal source (most commonly alkali hydroxide and/or alkali silicate solutions) (Buchwald et al., 2003; Shi et al., 2006). The resulting material is a binder system cured at room

temperature with mechanical properties and durability potentially suitable for Portland cement replacement. The supply of an alkali metal source via an alkaline solution raises the pH of the reaction mixture and accelerates the dissolution of the aluminosilicate powder. Its dissolution releases some of its constitutive elements into the medium that combine with the ions of the alkaline solution to form a binding phase. Different binding phases are formed depending on the nature of ions dissolved from the aluminosilicate source. For example, the binding phase consists of Calcium Silicate Hydrate (as in Portland cement) if the ion released by the aluminosilicate source is calcium and consists of a three-dimensional aluminosilicate network known as a geopolymer binder if the ions released by the aluminosilicate source are mainly silicon and aluminium.

3 Materials and methods

3.1 *Materials*

A Polish fly ash derived from hard coal and coal slime combustion in fluidised bed boiler was used in this study. It consists primarily of SiO_2, Al_2O_3 and CaO (Table 1). The fly ash contains 52% of particles sized lower than 45 μm and 41% lower than 10 μm. Speswhite kaolin provided by Imerys Minerals UK was also used in this study (Table 1). It is mainly constituted of kaolinite (95%) and secondarily of muscovite (4%) (Chemeda, 2015). The kaolin contains, approximately, 100 % of particles sized lower than 10 μm and 80 % lower than 2 μm. Its specific gravity is $G_s = 2.60$. The liquid and plastic limits are 70 % and 32 % respectively giving a plasticity index of 38 % (Vitale et al., 2016).

The alkaline solution used consisted of a sodium silicate with a molar ratio SiO_2/Na_2O of 1.7, dry mass percentage of 44%, and density of 1.55g/cm³ (supplied by Woellner Group and under the commercial name GEOSIL 34417).

3.2 Sample preparation

Sample preparation was designed to mimic the process that would be adopted in embankment construction. The alkaline solution (sodium silicate and water) was stirred for one hour and then sprayed on the mix of aluminosilicate (fly ash) and kaolin powders previously mixed together. Kaolin and fly ash were mixed in proportion 90/10 by dry mass (mix referred to as KF10). This ratio is in line with the fraction of Portland cement typically added to soil to be stabilised (in the range 7 to 12 % according to Petry and Wohlgemuth, 1988).

The wet powder was statically compacted to a vertical stress of 600 kPa (maintained for 1h). Once the compaction load was removed, the samples were cured for 1, 7, 14, 28, 60 or 90 days at 20 °C inside their moulds. Finally, samples within their mould were stored under vacuum to avoid carbonation during curing.

The mould was the oedometer ring for samples to be tested in one-dimensional compression and a purposely designed 3D printed plastic mould for samples to be tested in direct shear tests. This plastic mould was designed in order to cure several samples simultaneously while using a single shear box for testing. It was designed in Autodesk Fusion 360 and printed with the Ultimaker 2 Extended 3D printer. The mould was made of lower and upper halves kept together by screws (Fig. 1). It was initially designed to directly serve as the lower and upper halves of the shear box. However, the plastic frames were not used to test the samples, which were indeed transferred from the mould to the metal lower and upper halves of the direct shear box.

The initial water content was fixed to 28% for all the samples, which corresponds to the optimum moisture content determined by Proctor compaction test (Sivakumar and Wheeler, 2000). Additionally, the mass ratio of alkaline solution to fly ash was fixed to

50%, giving the initial molar ratios (considering that kaolin is unreactive): Si/Al = 1.2, Si/Na = 2.7 and Al/Na = 2.1. It is worth noticing that the Al/Na ratio was not fixed to one, which is the value that optimises the properties of alkali activated materials. The ratio Al/Na =1 is adequate to provide a charge-balancing of the negative AlO_4^- tetrahedron charge but not in excess to promote efflorescence that may disrupt the polymerisation process (Barbosa et al., 2000). In the case examined in this work, the presence of calcium ions in high quantity plays a role of charge compensation as well as sodium and this is the reason for accepting an Al/Na ratio different from one.

3.3 Methods

3.3.1 One-dimensional compression test

Oedometer tests were performed on compacted samples in standard oedometer cell. After saturation by filling the external container with water, vertical stress σ_v was applied in steps ($\Delta\sigma_v/\sigma_v = 1$) up to 2220 kPa and then reversed. Samples were allowed to consolidate under each loading. As consolidation time t_{100} was of the order of a few minutes, total test duration could be maintained within 1 day thus avoiding significant curing inside the oedometer cell.

3.3.2 Direct shear test

Direct shear tests were performed according to ASTM D 3080-90 (ASTM D 3080-90, 1994) on compacted samples in a standard shear box. Cured samples were transferred to the shear box by centring the 3D printed mould onto the shear box upper half and pushing down the sample using a load frame with the help of a wooden pusher. Samples were fully saturated by filling the external container with water and vertical displacements were monitored. After saturation, a normal stress of 100 kPa was applied in steps until full

consolidation was achieved. Shear displacements were then applied at a rate of 0.04 mm/min.

3.3.3 Mercury Intrusion Porosimetry (MIP)

MIP tests were carried out on samples removed from the oedometer cell at a given vertical stress in order to capture microstructural features of samples induced by loading along the compressibility curve. MIP tests were performed on freeze dried samples by a double chamber Micromeritics Autopore III apparatus. In the filling apparatus (dilatometer) samples were outgassed under vacuum and then filled by mercury allowing increase of absolute pressure up to ambient one. Using the same unit, the intrusion pressure was than raised up to approximately 200 kPa by means of compressed air. The detected pore-entrance sizes ranged between 134 μm and 7.3 μm (approximately 0.01 MPa - 0.2 MPa for a mercury contact angle of 139°). After depressurisation to ambient pressure, samples were transferred to high-pressure unit, where mercury pressure was increased up to 205 MPa following a previously set intrusion program. The smallest detected entrance pore diameter was about 7 nm. Corrections to pore-size distribution due to compressibility of intrusion system were applied performing a blank test.

Samples tested in the MIP were obtained by imposing a vertical stress of either 714 or 1428 kPa. Two different samples for each stress level were prepared, as suggested by Pedrotti and Tarantino (2018). After reaching the target applied stress, the first sample was quickly unloaded in one single step to minimise recovering of volumetric strains (undrained conditions). The sample was then rapidly removed from the oedometer and sealed in plastic bag to prevent water loss until the freeze-drying was performed. This sample will be referred to as '*ncl*' as it was expected to maintain the microstructure of the material along the normal compression line. The second sample was unloaded under

drained conditions, allowing the rebound of the structure and the recovering of elastic strains. This sample will be referred to as '*url*' as it was expected to maintain the microstructure of the material along the unloading-reloading line.

4 Results

4.1 One-dimensional compression

Fig. 2 shows compressibility curves of the raw kaolin and the treated kaolin (KF10) as a function of curing period. The samples with curing period of 1d and 7d show very similar initial void ratio (following saturation) as the raw kaolin. Upon loading, the material KF10 maintains a higher void ratio although the normal compression line attained eventually appears to be parallel to the one of the raw kaolin (in a semi-log scale).

The sample with curing period of 14 days shows an initial void ratio (after saturation) lower than raw kaolin and the KF10 samples cured for 1 and 7 days. However, its compression curve re-joins the curves of samples cured for 1 and 7 days at 357 kPa.

The samples with curing periods of 28, 60, and 90 days also show an initial lower void ratio. The compression curves are very similar and show a normal compression branch higher than the one of the samples cured for 1, 7, and 14 days (although the normal compression lines still appears to be parallel to the ones of samples cured for 1, 7, and 14 days).

The unloading curves are consistent with the loading behaviour. The samples with curing period of 1, 7, and 14 days, which presented similar behaviour in loading, also show similar response in unloading and are stiffer than raw kaolin. The samples with curing period of 28, 60, and 90 days, which presented similar behaviour in loading, also show

similar response in unloading and stiffer response than samples cured for 1, 7, and 14 days.

Overall, the response in compression for short curing period (1 and 7 days) appears significantly different from the one observed for long curing periods (28, 60, and 90 days). The sample cured for 14 days shows intermediate behaviour.

4.2 Pore-size distribution (PSD)

To investigate the effect of loads on the microstructure of the treated soil, mercury intrusion porosimetry analyses were performed at 28 days on treated samples subjected to either 714 or 1428 kPa. As shown in Fig. 2, the 714 kPa stress is approximately associated with the yielding stress whereas the 1428 kPa stress is associated with a post-yielding stress state.

The pore-entrance size frequency distributions before and after unloading are shown in Fig. 3. Samples show a bimodal distribution of entrance pore diameters. As widely accepted (e.g. Delage et al., 1996; Tarantino and De Col, 2008; Russo and Modoni, 2013), microstructure of compacted treated samples is characterized by an aggregate structure, with smaller pores (associated with modal size of ~0.18 μm) corresponding to intra-aggregates pores and larger pores (associated with modal size in the range 0.6-1.0 μm) corresponding to inter-aggregates pores.

The most significant changes of microstructure induced by the applied load occurs in the inter-aggregate porosity with a shift of the larger pores (0.4 μm – 10 μm) towards smaller pore sizes (Fig. 3a). This shift remains when samples are unloaded (Fig. 3b) indicating that non-reversible deformation is associated with the change in inter-aggregate porosity,

possibly associated with partial destructuration. On the other hand, the intra-aggregate pores do not appear to be affected by the applied loads.

The changes of microstructure associated with the unloading process show a similar pattern, i.e. only the inter-aggregate porosity is affected by the rebound whereas the intra-aggregate pores remain unchanged upon unloading (Fig. 3b,c).

4.3 Shear strength

Fig. 4 shows the shearing behaviour of the raw kaolin and the fly ash-based alkali activated binder treated soil KF10 as a function of curing period for normal stresses of 100 and 200 kPa respectively. All samples show contractive behaviour upon shearing regardless of the normal stress applied and curing period.

At 100 kPa normal stress (Fig. 4a), the alkali activated treated samples KF10 at 1 and 7 days display a very similar behaviour suggesting that chemical reactions have not yet taken place in such a short period. Nonetheless, the mobilised shear stress appears to be higher than the raw kaolin. At 28-day curing time, the sample appears to be stiffer, shows a clear peak, and an ultimate shear strength higher than the samples cured for 1 and 7 days.

At 200 kPa normal stress (Fig. 4b), the alkali activated treated samples KF10 at 7 days shows a mobilised shear strength higher than the raw kaolin in the shear displacement range 0-4mm and then appears to converge to the raw kaolin curve at very large shear displacements. In contrast, the sample characterised by 28-day curing time exhibits a mobilised shear strength always higher than the raw kaolin sample and the sample cured for 7 days.

Normal displacements did not always level off at large shear displacements. Data were therefore replotted by correcting the shear to normal stress ratio τ/σ' for dilatancy $\Delta y/\Delta x$, where y and x are the normal and shear displacements respectively. Fig. 5 shows all the tests at 100 kPa normal stress. Samples cured for 1 and 7 days show higher mobilised shear stress in the low/medium range of shear displacements whereas the curves tend to converge to the raw kaolin at high shear displacements. On the other hand, the sample cured for 28 days shows significant gain with respect to the raw kaolin even at large shear displacements. At large displacements, the stress ratio varies from ~0.4 for raw kaolin to ~0.55 for KF10 cured for 28 days, corresponding to angles of shearing resistance equal to 22° and 29° respectively.

Fig. 6 compares the stress-displacement curves at 100 and 200 kPa normal stress (for 7 and 28 days curing periods). At large displacements, the curves at 100 and 200 kPa normal stress converge suggesting that the KF material does not exhibit any effective cohesion *c*' in this range of normal stress for both curing periods. Fig. 6 also shows that the sample cured for 28 days exhibit peak shear strength only when tested at the lower normal stress (100 kPa) and this peak essentially disappears when the normal stress is increased to 200 kPa. Finally, Fig. 6 confirms that there is substantial gain of shear strength as curing period increases from 7 to 28 days.

5 Discussion

This study aimed to address four research questions i) does the alkali-activated calcium-rich fly ash enhance significantly the mechanical performance of 'marginal' clay geomaterials, ii) what is the timescale of the physicochemical processes activated by the alkaline solution and their effects on the mechanical response of the treated clay, iii) what

are the mechanisms at the particle/aggregate scale controlling the macroscopic behaviour of the treated clay, and iv) what are the engineering applications where this stabilisation can be successfully envisaged. The first question is clearly answered by the oedometer and direct shear tests results (Fig. 2 and Fig. 4 to Fig. 6), i.e. the addition of alkali activated fly ash increases significantly stiffness and shear strength at least in certain stress ranges.

5.1 Timescale of binding phase formation

Fig. 7a shows the ^{29}Si MAS-NMR spectrum for the fly ash alone compared with the spectra of the fly ash following alkali activation (after 28 days and 6 months). The appearance of a new resonance located at -85 ppm is associated with the formation of the binding phase and it corresponds to Q^2-type silicon environments in chain structure that resembles the one of Calcium Silicate Hydrates encountered in Portland Cement (Coudert et al., 2018, Coudert et al., 2021). From 28 days to 6 months, the resonance associated with the binding phase does not change neither in amplitude nor in chemical shift value indicating a negligible evolution of the binding phase in terms of both chemistry and atomic structure beyond 28 days.

Fig. 7b shows the ^{29}Si MAS-NMR spectra for kaolinite mixed with 50% of fly ash (KF50) at 1 day, 28 days, and 6 months (spectrum of the alkali activated fly ash alone at 28 days is also shown for reference). The formation of the new resonance located at -85 ppm associated with the binding phase is only present at 28 days and 6 months but not after 1 day, indicating that the binding phase does not yet form in such a short time lag. Fig. 7b also shows that the resonance associated with kaolinite at -91 ppm does not undergo any modification over time suggesting that the kaolinite has no reactivity. Although Fig. 7b shows the spectra for KF50 mixture (50% flay ash fraction), similar pattern should be

expected for the KF10 mixture (10% flay ash fraction) tested in the experimental programme presented herein.

5.2 Micro-scale mechanisms

The one-dimensional compression tests Fig. 2 have shown three distinct behaviours. The raw kaolin shows an almost immediate transition to a normally consolidated state (compression curve liner in a semi-log plot). According to Pedrotti and Tarantino (2018), this would be associated with the progressive disengagement of edge-to-face contacts of the initially 'flocculated' fabric occurring at pH values lower the point of Zero Charge (PZC).

In contrast, the treated clay in the very short term (days 1 and 8 following the alkali activation) shows an over-consolidated behaviour and a transition to normally consolidated state in the range 357-714 kPa. Since the binding phase does not form yet after 1 day (Fig. 7b) and the compression curves after 1 and 8 days are very similar (Fig. 2), it can be inferred that the binding phase does not form even after 8 days. As a result, the different compression behaviour observed for the treated kaolinite after 1 and 8 days compared to the kaolinite alone would not be due to the formation of the binding phase but should be sought in the change of pore-water chemistry due to the addition of the alkaline solution.

The alkaline environment generated by the addition of the sodium silicate aqueous solution makes the kaolinite particles charged negatively on both edge and basal planes (Wang and Siu 2006) thus preventing the formation of aggregates by edge-to-face association (flocculated fabric). In kaolinite with negligible electrolyte concentration, this would generate a 'dispersed' fabric with significant reduction in void ratio compared with

clay in acidic environment (Pedrotti and Tarantino, 2018). The increase in pH would therefore cause a reduction in void ratio rather than an increase as observed in Fig. 2.

The higher void ratio of the KF10 material cured for 1 and 8 days observed over the entire stress range can only be justified by clay particles forming stacks promoted by the reduced double-layer repulsion in turn induced by the increase of electrolyte concentration associated with the addition of the alkaline solution (electrolyte concentration would be of the order of 1 molal if Na_2O dissociated completely in water). This is in line with the observations by Vitale et al. (2016) who analysed the effect of addition of CaO that, similarly to Na_2O, also increases both pH and electrolyte concentration.

At high stress, the slope of the normal consolidation line (ncl) becomes parallel to the one of clay alone suggesting similar micro-mechanisms ruling non-reversible behaviour. It can be speculated that stacks are orienting similarly to individual particles for the case of clay alone (Fig. 8).

In the long term (after 28, 60, and 90 days) the binding phase has formed (Fig. 7b) and this generates a further increase in the pre-consolidation stress (Fig. 2) possibly due to the bonding of the aggregates. The normal compression line (ncl) remains parallel to the one measured for samples cured for 1 and 8 days suggesting similar mechanisms for non-reversible deformation. It can therefore be speculated that the bonds are broken at high stresses and the higher void ratio is simply due to the presence of an additional phase filling the pore space.

The assumption about the aggregate fabric forming in the treated clay can be corroborated by pore-size distribution data. Fig. 9 shows the pore-size distributions of the samples KF10 loaded to 714 and 1428 kPa respectively. These distributions are clearly bi-modal with modal sizes of ~0.15 and ~1 μm respectively. The same figure also shows pore-size

distributions of different 'untreated' kaolinite samples, two samples compacted to 1200 kPa vertical stress at water contents of 0.10 and 0.24 respectively and then saturated and one sample reconstituted from slurry and loaded to 70 kPa vertical stress (after Pedrotti, 2016). Despite the very different sample preparation procedures and hydro-mechanical history, it can be observed that saturated kaolinite alone always exhibits a mono-modal distribution with modal size ~0.25 μm. As a result, the bi-modal distribution of the treated samples as compared to the mono-modal distribution of saturated kaolinite alone corroborates the assumption of aggregated fabric for the treated kaolin.

The conceptual microstructural model laid down in Fig. 8 with reference to 1D compression behaviour can also explain the effect of alkaline activation on shear strength. In the short term (1 and 8 days), the aggregation induced by the change in pore-water chemistry would explain the higher shear strength of the treated kaolinite compared to the raw kaolinite in the intermediate horizontal displacement range (Fig. 5). At large horizontal displacements, the effect of aggregation seems to be lost, which is in line with the compressibility of the treated clay at 1 and 8 days recovering the same values of the compressibility of the raw kaolinite at high compression stresses (Fig. 2).

In the long term (28 days), the binding phase generates an increase in shear strength over the entire displacement range with both peak and ultimate shear strength significantly enhanced by the formation of the binding phase (Fig. 6). It is worth noticing that the treated clay experienced no dilatancy upon shearing (Fig. 4a). Peak shear strength is therefore associated with the presence of the binding phase. The decay of shear strength following peak in the sample tested at 100 kPa normal stress at 28 days is likely associated with partial breakage of the binding phase. This peak does not appear in the sample tested

at 200 kPa normal stress at 28 days likely because the higher normal stress facilitates earlier breakage of the binding phase.

5.3 Engineering applications

Results from 1D compression tests show that there is an immediate increase in stiffness following alkaline activation in the stress range 10-700 kPa and this effect is enhanced in the long term once the binding phase forms. On the other hand, the beneficial effects in stiffness is lost at very high stress. This makes alkali activated fly ash a suitable binder for stabilisation of marginal clays, alternative to traditional binders such as lime and/or cement. The range of stresses where this improvement technique appears to be effective well fits the typical range of stresses in embankments or earthfills, suggesting it could be applied successfully to enhance the performance of several geotechnical structures involving compaction of marginal geomaterials.

6 Conclusions

This paper has examined the use of a calcium-rich fly ash from coal combustion activated by a sodium-based alkaline solution for the treatment of non-active clay in view of its use as earthfill geomaterial.

When subjected to one-dimensional compression, the treated soil shows an increase in-pre-consolidation stress and, hence, an increase in stiffness in the stress range up to ~700 kPa. This increase is observed even in the very short-term (1 day after alkali activation), i.e. before the binding phase starts to form. This was attributed to the changes in pore-water chemistry following the addition of the alkaline solution. The increase in electrolyte concentration is assume to deplete the double-layer repulsion and promote aggregation in

face-to-face mode. The aggregated fabric of the treated kaolin was confirmed by pore-size distribution data from mercury intrusion porosimetry. In the long term (curing time ≥28days) stiffness appeared to be further enhanced due to the formation of the binding phase.

Peak shear strength also appeared to be significantly enhanced in both short and long term although effects were more pronounced for curing time ≥28days following the formation of the binding phase. Ultimate shear strength appeared to be enhanced only in the long term (curing time ≥28days) due to the presence of the binding phase creating bonding between clay particles. For short curing periods, the change of pore-water chemistry does not seem to affect the ultimate shear strength possibly due to the aggregates breaking down. This study confirms the potential of fly ash-based alkali activated binder for stabilisation of clay to be used as compacted earthfill material.

Acknowledgements

The authors wish to acknowledge the support of the European Commission via the Marie Skłodowska-Curie Innovative Training Networks (ITN-ETN) project TERRE 'Training Engineers and Researchers to Rethink geotechnical Engineering for a low carbon future' (H2020-MSCA-ITN-2015-675762).

References

Askeland, D.R., Fulay, P.P., Wright, W.J., 2011. The science and engineering of materials, 6th ed. ed. Cengage Learning, Stamford, CT.

ASTM D 3080-90, 1994. Standard test method for direct shear test of soils under consolidated drained conditions. Annu. Book ASTM Stand. 04.08., 290–295.

Barbosa, V. F., MacKenzie, K. J.D., Thaumaturgo C. 2000. Synthesis and characterisation of materials based on inorganic polymers of alumina and silica: sodium polysialate polymers. International Journal of Inorganic Materials 2, no. 4 pp. 309–17

Buchwald, A., Kaps, C., Hohmann, M., 2003. Alkali-activated binders and pozzolan cement binders–complete binder reaction or two sides of the same story, in: Proceedings of the 11th International Conference on the Chemistry of Cement. Portland Cement Association Durban, South Africa, pp. 1238–1246.

Chemeda, Y., 2015. Effect of hydrated lime on kaolinite surface properties and its rheological behaviour. PhD Thesis, Université de Nantes, France.

Coudert, E., Paris, M., Deneele, D., Russo, G., Tarantino, A., 2018. Use of alkali activated fly ash binder for kaolin clay soil stabilisation: Physicochemical evolution. Construction and Building Materials 201 (2019) 539–552

Coudert, E., Deneele, D., Russo, G., Vitale, E., Tarantino, A., 2021. Microstructural evolution and mechanical behaviour of alkali activated fly ash binder treated clay. Construction and Building Materials 285 (2021) 122917.

Cristelo, N., Glendinning, S., Fernandes, L., Pinto, A.T., 2012. Effect of calcium content on soil stabilisation with alkaline activation. Constr. Build. Mater. 29, 167–174. https://doi.org/10.1016/j.conbuildmat.2011.10.049

Cristelo, N., Glendinning, S., Teixeira Pinto, A., 2011. Deep soft soil improvement by alkaline activation. Proc. Inst. Civ. Eng. - Ground Improv. 164, 73–82. https://doi.org/10.1680/grim.900032

Delage, P., Audiguier, M., Cui, Y.-J., Howat, M.D., 1996. Microstructure of a compacted silt. Can. Geotech. J. 33, 150–158. https://doi.org/10.1139/t96-030

Head, K.H., 1994. Manual of Soil Laboratory Testing Volume 2: Permeability, Shear Strength and Compressibility Tests. Second Edition, ELE International Limited.

Pedrotti, M. 2016. An experimental investigation on the micromechanics of non-active clays in saturated and partially-saturated states. PhD thesis, University of Strathclyde, Glasgow, UK.

Pedrotti, M., Tarantino, A., 2018. An experimental investigation into the micromechanics of non-active clays. Géotechnique 68(8): 666-683

Petry, T., and Wohlgemuth, S. K. 1988. The Effects of Pulverization on theStrength and Durability of Highly Active Clay Soil Stabilized with Limeand Portland Cement. In Transportation Research Record 1190, TRB, National Research Council, Washington, D.C., pp. 38–45.

Provis, J.L., van Deventer, J.S.J. (Eds.), 2014. Alkali Activated Materials, RILEM State-of-the-Art Reports. Springer Netherlands, Dordrecht.

Rios, S., Cristelo, N., Viana da Fonseca, A., Ferreira, C., 2016. Structural Performance of Alkali-Activated Soil Ash versus Soil Cement. J. Mater. Civ. Eng. 28, 4015125. https://doi.org/10.1061/(ASCE)MT.1943-5533.0001398

Russo, G., Modoni, G., 2013. Fabric changes induced by lime addition on a compacted alluvial soil. Géotechnique Lett. 3, 93–97. https://doi.org/10.1680/geolett.13.026

Scrivener, K.L., Kirkpatrick, R.J., 2008. Innovation in use and research on cementitious

material. Cem. Concr. Res. 38, 128–136. https://doi.org/10.1016/j.cemconres.2007.09.025

Shi, C., Krivenko, P.V., Roy, D.M., 2006. Alkali-activated cements and concretes. Taylor & Francis, London ; New York.

Silva, R.A., Oliveira, D.V., Miranda, T., Cristelo, N., Escobar, M.C., Soares, E., 2013. Rammed earth construction with granitic residual soils: The case study of northern Portugal. Constr. Build. Mater. 47, 181–191. https://doi.org/10.1016/j.conbuildmat.2013.05.047

Singhi, B., Laskar, A.I., Ahmed, M.A., 2016. Investigation on Soil–Geopolymer with Slag, Fly Ash and Their Blending. Arab. J. Sci. Eng. 41, 393–400. https://doi.org/10.1007/s13369-015-1677-y

Sivakumar, V. & Wheeler, S. J. 2000. Influence of compaction procedure on the mechanical behaviour of an unsaturated compacted clay. Part 1: Wetting and isotropic compression. Geotechnique 50, No. 4, 359–368.

Tarantino, A., De Col, E., 2008. Compaction behaviour of clay. Géotechnique 58, 199–213.

Tenn, N., Allou, F., Petit, C., Absi, J., Rossignol, S., 2015. Formulation of new materials based on geopolymer binders and different road aggregates. Ceram. Int. 41, 5812–5820. https://doi.org/10.1016/j.ceramint.2015.01.010

Vitale, E., Deneele, D., Russo, G., Ouvrard, G., 2016. Short-term effects on physical properties of lime treated kaolin. Appl. Clay Sci. 132–133, 223–231. https://doi.org/10.1016/j.clay.2016.04.025

Wang, Y. H. & Siu, W. K. (2006). Structure characteristics and mechanical properties of kaolinite soils. I. Surface charges and structural characterizations. Can. Geotech. J.

43, No. 6, 587–600.

Wilkinson, A., Haque, A., Kodikara, J., 2010. Stabilisation of clayey soils with industrial by-products: part A. Proc. Inst. Civ. Eng. - Ground Improv. 163, 149–163. https://doi.org/10.1680/grim.2010.163.3.149

TABLE LEGENDS

Table 1. Chemical composition (wt. %) of raw fly ash and kaolin.

Table 2. Comparison of void ratio *e* determined by oven-drying and void ratio e_{MIP} measured by mercury intrusion porosimeter.

FIGURE LEGENDS

Fig. 1. 3D printed mould (A) design of the base, (B) design of the cover and (C) assemblage of the mould.

Fig. 2. One-dimensional compression tests on kaolin and alkali activated binder treated kaolin (KF10) at different curing periods.

Fig. 3. Frequency distribution of entrance pore size for alkali activated fly ash binder treated soil KF10 at 28-day curing period (ncl=samples unloaded under undrained conditions; url=samples unloaded under drained conditions). (a) Samples loaded to 714 and 1428 kPa. (b) Samples unloaded from 714 and 1428 kPa. (c) Samples loaded to and unloaded from 714 kPa. (d) Samples loaded to and unloaded from 1428 kPa.

Fig. 4. Direct shear tests on kaolin and alkali activated binder treated kaolin (KF10) at different curing periods. (a) normal stress σ=100 kPa. (b) normal stress σ=200 kPa

Fig. 5. Direct shear tests on kaolin and alkali activated binder treated kaolin (KF10) at different curing periods and normal stress σ=100 kPa: shear strength data corrected for dilatancy.

Fig. 6. Direct shear tests on kaolin and alkali activated binder treated kaolin (KF10) at at curing periods 7 and 28 days and normal stresses σ=100 kPa and σ=200 kPa: shear strength data corrected for dilatancy.

Fig. 7. ^{29}Si MAS-NMR spectra. (a) Raw fly ash and binder F100 at 28 days and 6 months. (b) alkali activated binder F100 at 28 days and alkali activated kaolin KF50 at 1 and 28 days (after Coudert et al., 2019).

Fig. 8. Conceptual model for micro-mechanical behaviour of raw kaolin and alkali activated fly ash binder treated clay.

Fig. 9. Frequency distribution of entrance pore size for alkali activated fly ash binder treated soil KF10 at 28-day curing period compared with kaolin samples i) compacted to 1200 kPa normal stress at water contents of 10% and 24% and then saturated and ii) sample reconstituted from slurry and loaded to 70 kPa normal stress (after Pedrotti 2016)

TABLES

Table 1. Chemical composition (wt. %) of raw fly ash and kaolin.

	SiO_2	Al_2O_3	Fe_2O_3	CaO	CaO_{free}[a]	MgO	SO_3	Na_2O	K_2O	H_2O	L.o.I.
Fly ash	39.4	19.8	7.4	18.6	5.2	1.8	4.1	2.0	1.8	0.0	1.7[b]
Kaolin	49.2	34.5	1.2	0.0	0.0	0.2	0.0	0.1	1.7	13.1	12.0[c]

[a] Free calcium oxide content
[b] L.o.I = Loss on ignition 900 °C
[c] L.o.I = Loss on ignition 1000 °C

Table 2. Comparison of void ratio *e* determined by oven-drying and void ratio e_{MIP} measured by mercury intrusion porosimeter.

	e	e_{MIP} – ncl	e_{MIP} – url
KF10 - 28 days - 714 kPa	1.22	1.48	1.58
KF10 - 28 days - 1428 kPa	1.10	1.41	1.39

FIGURES

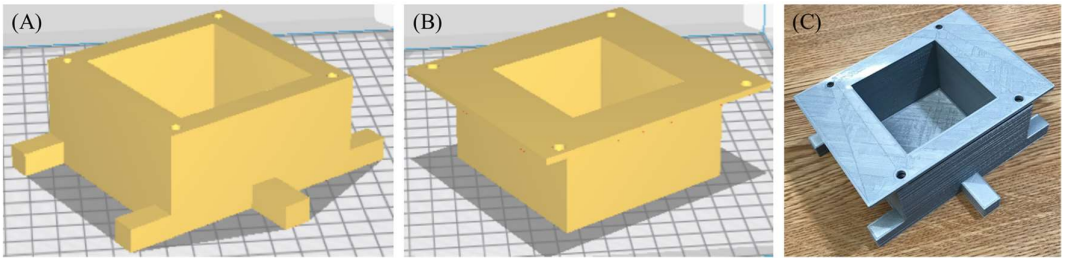

Fig. 1. 3D printed mould (A) design of the base, (B) design of the cover and (C) assemblage of the mould.

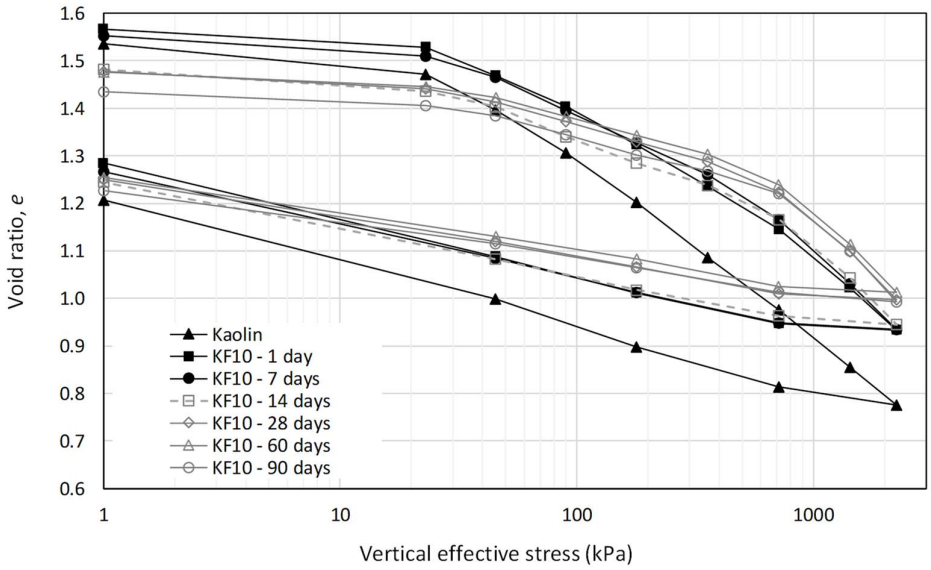

Fig. 2. One-dimensional compression tests on kaolin and alkali activated binder treated kaolin (KF10) at different curing periods.

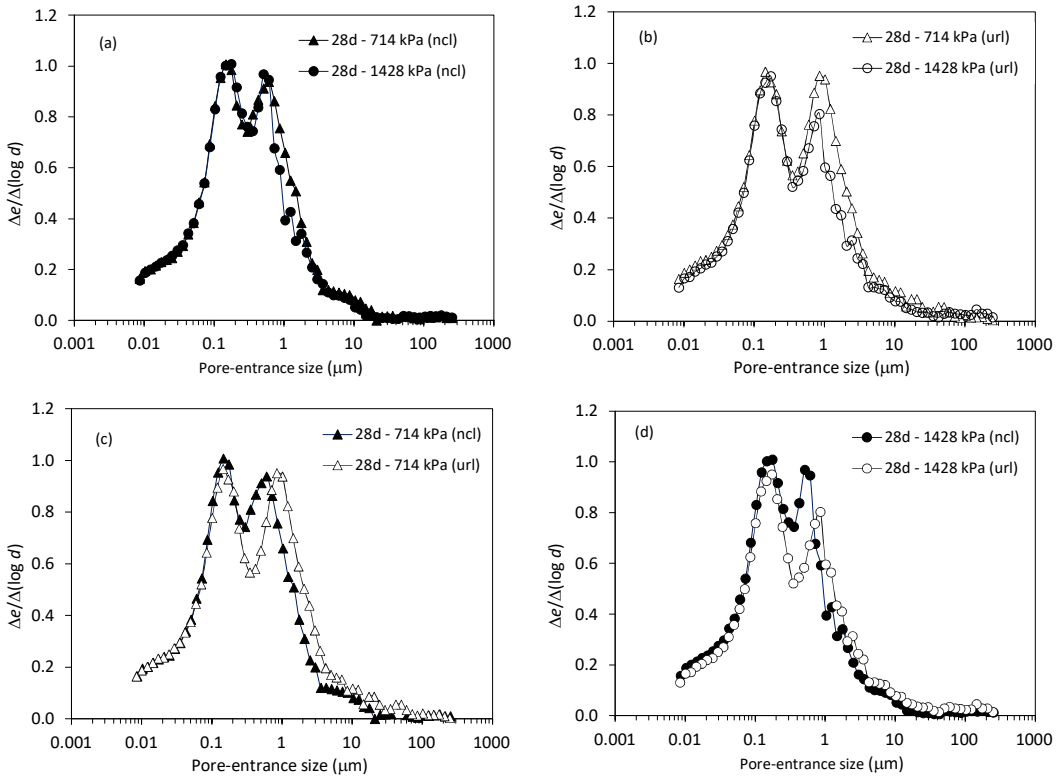

Fig. 3. Frequency distribution of entrance pore size for alkali activated fly ash binder treated soil KF10 at 28-day curing period (ncl=samples unloaded under undrained conditions; url=samples unloaded under drained conditions). (a) Samples loaded to 714 and 1428 kPa. (b) Samples unloaded from 714 and 1428 kPa. (c) Samples loaded to and unloaded from 714 kPa. (d) Samples loaded to and unloaded from 1428 kPa.

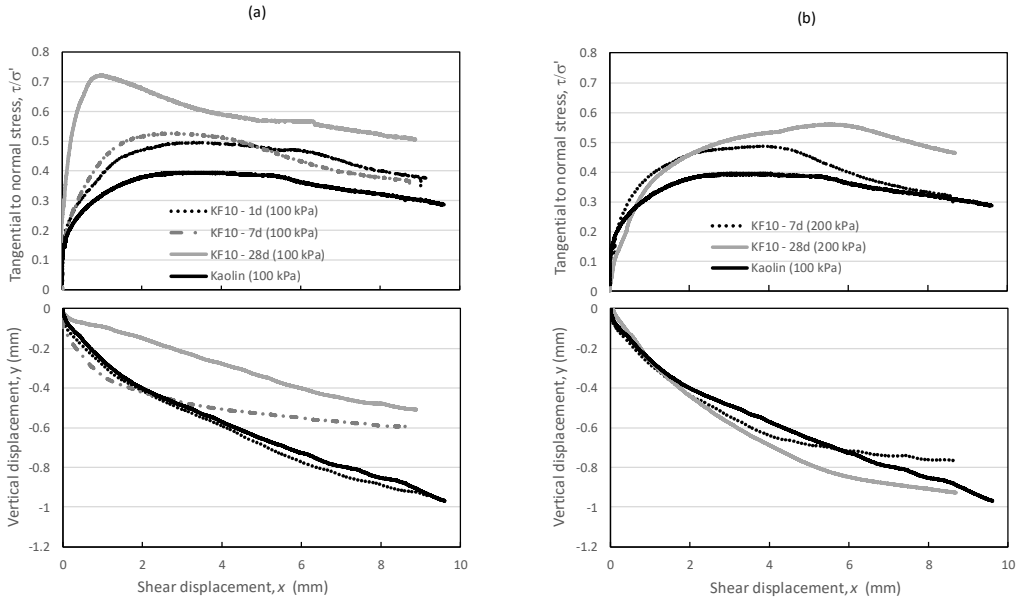

Fig. 4. Direct shear tests on kaolin and alkali activated binder treated kaolin (KF10) at different curing periods. (a) normal stress σ=100 kPa. (b) normal stress σ=200 kPa

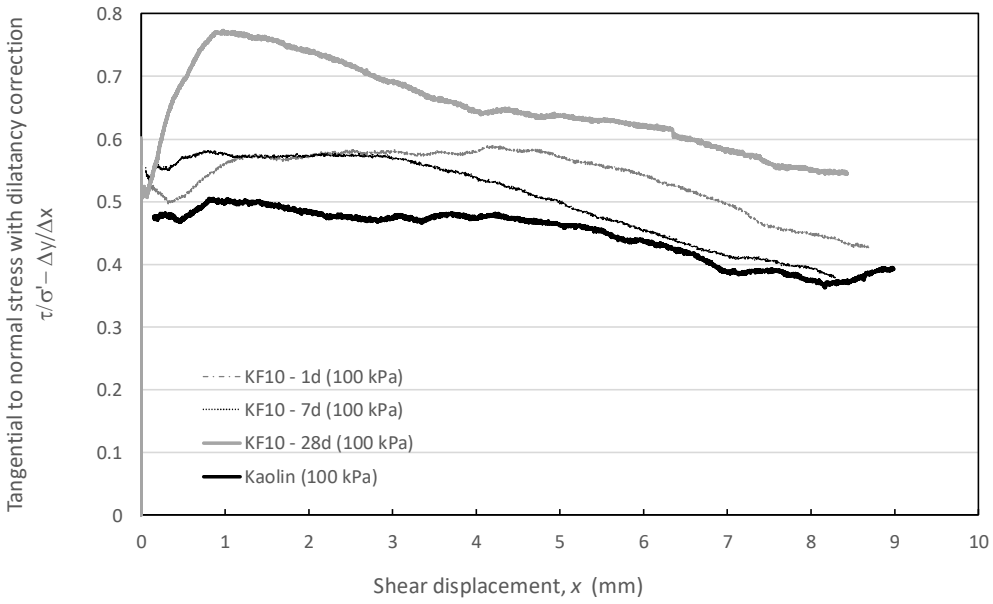

Fig. 5. Direct shear tests on kaolin and alkali activated binder treated kaolin (KF10) at different curing periods and normal stress σ=100 kPa: shear strength data corrected for dilatancy.

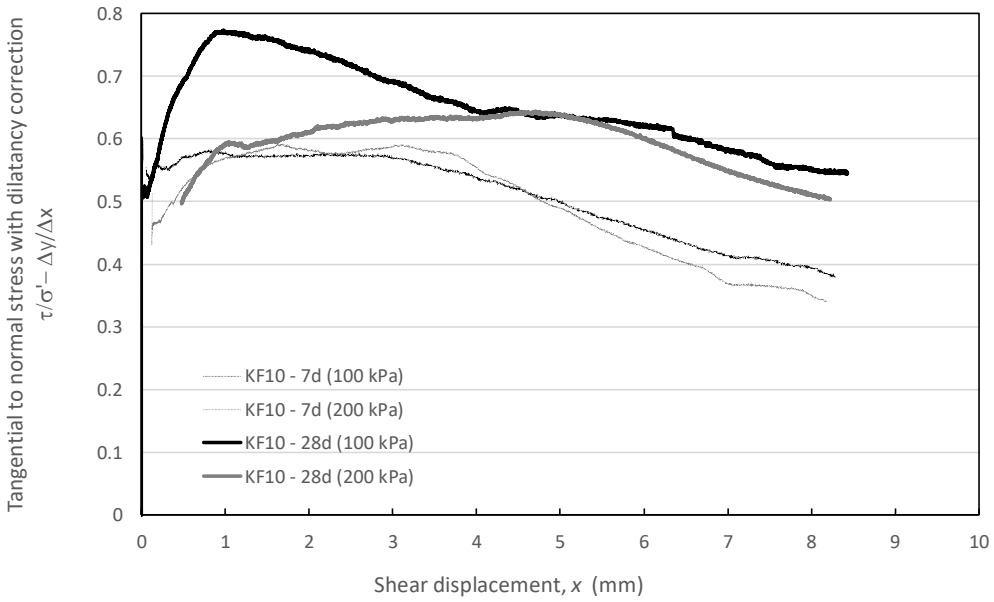

Fig. 6. Direct shear tests on kaolin and alkali activated binder treated kaolin (KF10) at at curing periods 7 and 28 days and normal stresses σ=100 kPa and σ=200 kPa: shear strength data corrected for dilatancy.

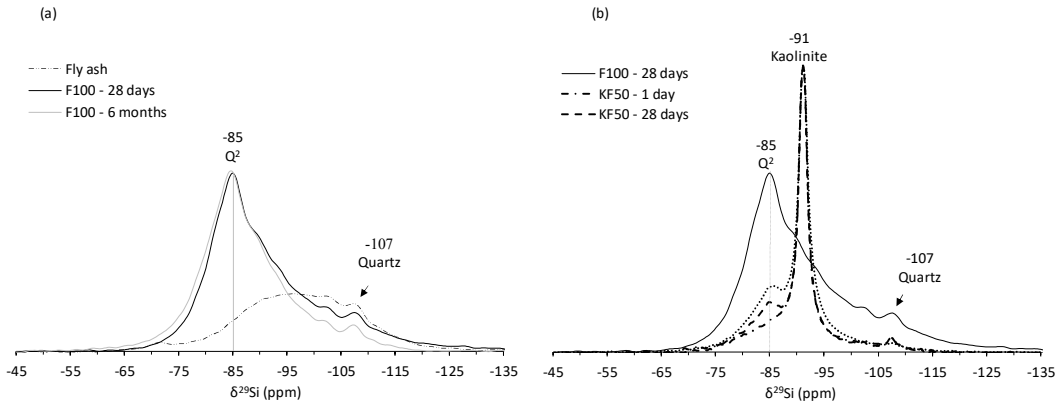

Fig. 7. ^{29}Si MAS-NMR spectra. (a) Raw fly ash and binder F100 at 28 days and 6 months. (b) alkali activated binder F100 at 28 days and alkali activated kaolin KF50 at 1 and 28 days (after Coudert et al., 2019).

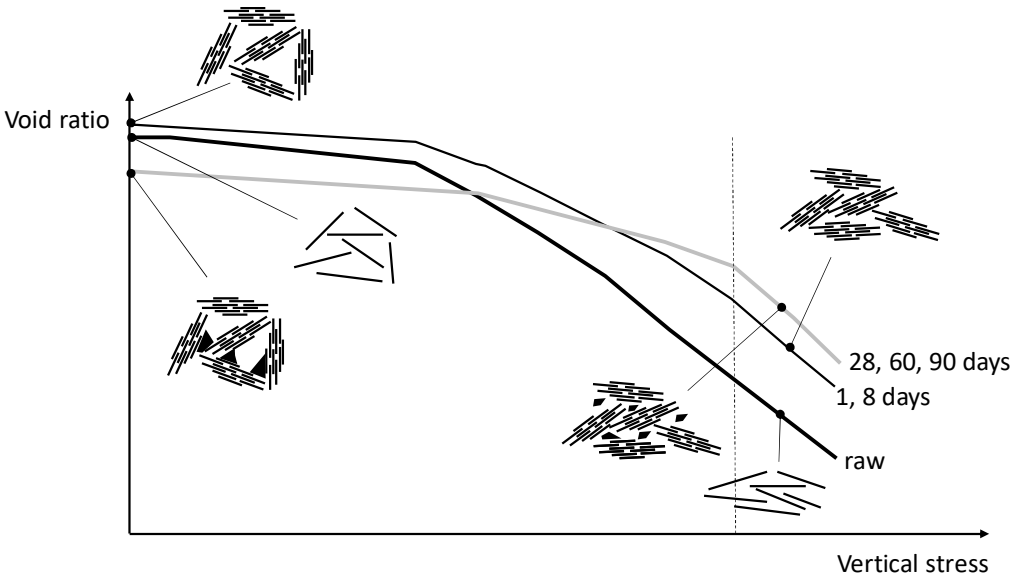

Fig. 8. Conceptual model for micro-mechanical behaviour of raw kaolin and alkali activated fly ash binder treated clay.

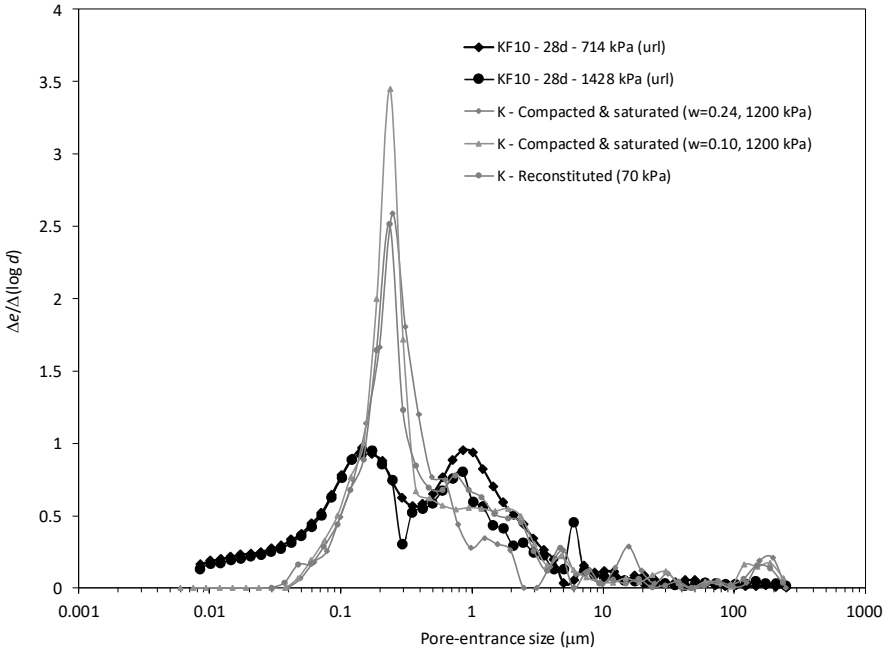

Fig. 9. Frequency distribution of entrance pore size for alkali activated fly ash binder treated soil KF10 at 28-day curing period compared with kaolin samples i) compacted to 1200 kPa normal stress at water contents of 10% and 24% and then saturated and ii) sample reconstituted from slurry and loaded to 70 kPa normal stress (after Pedrotti 2016)

Credit Author Statement

Author Contributions: Conceptualization and methodology, E.C., D.D., G.R., A.T.; investigation, E.C.; data curation, E.C., G.R., A.T.; writing—original draft preparation, E.C., G.R.; writing—review and editing, A.T., G.R.; supervision, G.R., A.T.

All Authors have read and agreed to the submitted version of the manuscript.